Pathways for Intracellular Generation of Oxidants and Tyrosine Nitration by a Macrophage Cell Line†

Amy M. Palazzolo-Ballance, Christine Suquet, and James K. Hurst*

Department of Chemistry, Washington State University, Pullman, Washington 99164-4630

Received January 21, 2007; Revised Manuscript Received April 19, 2007

ABSTRACT: Two transformed murine macrophage cell lines (RAW 264.7 ATCC TIB-71 and CRL-2278) were examined for oxidant production at various times following activation by using a set of fluorescence and ESR-active probes. Stimulation with a soluble agonist or activation with bacterial lipopolysaccharide plus γ-interferon caused only very small initial increases in O_2 consumption above basal rates; however, at 2−4 h post-activation, respiration increased to 2−3-fold and remained at these elevated levels over the subsequent lifetime of the cell (20−30 h). Oxidation reactions were confined primarily within the cell, as was demonstrated by using phagocytosable dichlorodihydrofluorescein-conjugated latex beads and cyclic hydroxylamines with differing membrane permeabilities. From the intrinsic reactivities of these probes and the time course of their oxidations, one infers the induction of apparent peroxidase activity beginning at ∼2 h post-activation coinciding with the increase in overall respiratory rate; this acquired capability was accompanied by accumulation of a stable horseradish peroxidase-reactive oxidant, presumably H_2O_2, in the extracellular medium. Nitrite ion rapidly accumulated in the extracellular medium over a period of 5−8 h post-activation in both cell lines, indicating the presence of active nitric oxide synthase (iNOS) during that period. Prostaglandin endoperoxide H synthase (COX-2) activity was detected at 15−20 h post-activation by the use of a sensitive peroxide assay in conjunction with a COX-2 specific inhibitor (DuP-697). Superoxide formation was detected by reaction with hydroethidine within the first hour following activation, but not thereafter. Consistent with the absence of significant respiratory stimulation, the amount of $O_2^{\bullet-}$ formed was very small; comparative reactions of cyclic hydroxylamine probes indicated that virtually none of the $O_2^{\bullet-}$ was discharged into the external medium. Myeloperoxidase (MPO) activity was probed at various times post-activation by using fluorescein-conjugated polyacrylamide beads, which efficiently trap MPO-generated HOCl in neutrophils to give stable chlorofluorescein products. However, chlorination of the dye was not detected under any conditions in RAW cells, virtually precluding MPO involvement in their intracellular reactions. This same probe was used to determine changes in intraphagosomal pH, which increased slowly from ∼6.5 to ∼8.2 over a 20 h post-phagocytosis period. The cumulative data suggest that activation is followed by sequential induction of an endogenous peroxidase, iNOS, and COX-2, with NADPH oxidase-derived $O_2^{\bullet-}$ playing a minimal role in the direct generation of intracellular oxidants. To account for reported observations of intracellular tyrosine nitration late in the life cycles of macrophages, we propose a novel mechanism wherein iNOS-generated NO_2^- is used by COX-2 to produce $NO_2^{\bullet}$ as a terminal microbicidal oxidant and nitrating agent.

The existence of motile phagocytic cells involved with host defense in higher organisms has been known since the discoveries of Metchnikoff in the early years of the last century (*1*). Extensive study on the neutrophil, in particular, has led to the recognition that both oxidative and nonoxidative reactions contribute to the microbicidal capabilities of these cells (*2*), although the physiological relevance of individual reactions remains unresolved and is an area of active investigation (*3*−*9*). In contrast, the microbicidal mechanisms of macrophages have received relatively little attention. Like the neutrophil, the macrophage possesses an NADPH oxidase (NOX-2)[1] that is activated upon agonist stimulation to form putative oxidative toxins initiated by the one-electron reduction of O_2 (*10*, *11*); however, unlike the

† This work was supported by a grant (AI-15834) to J.K.H. from the National Institute of Allergy and Infectious Diseases.

* Corresponding author. Phone: 509-335-7848. Fax: 509-335-8867. E-mail: hurst@wsu.edu.

[1] Abbreviations: NOX, NADPH oxidase; Amplex Red, 10-acetyl-3,7-dihydroxyphenoxazine; CMH, 1-hydroxy-3-methoxycarbonyl-2,2,5,5-tetramethylpyrrolidine; COX, prostaglandin endoperoxide H synthase; CPH, 1-hydroxy-3-carboxy-2,2,5,5-tetramethylpyrrolidine; DCF, 2,7-dichlorofluorescein; DCHF, 3,7-dichlorodihydrofluorescein; DMEM, Dulbecco's modified Eagle's medium; DTPA, diethylenetriaminepentaacetic acid; DTT, dithiothreitol; E^+, ethidium; HBSS, Hank's balanced salt solution; HE, hydroethidine; HRP, horseradish peroxidase; IFγ, mouse recombinant γ-interferon; LOX, lipoxygenase; LPS, bacterial lipopolysaccharide; MPO, myeloperoxidase; NMMA, *N*-methyl-L-arginine; NOS, nitric oxide synthase; 2-OH-E^+, 2-hydroxyethidium; PBS, phosphate-buffered saline; PMA, phorbol 12-myristate 13-acetate; PP•, 4-phosphono-oxy-2,2,6,6-tetramethylpiperidinyloxyl; PPH, 1-hydroxy-4-phosphono-oxy-2,2,6,6-tetramethylpiperidine; SOD, superoxide dismutase; XO, xanthine oxidase.

10.1021/bi700123s CCC: $37.00
Published on Web 05/27/2007

neutrophil, it lacks substantive myeloperoxidase (MPO) activity but contains an inducible nitric oxide synthase (iNOS) (*12*, *13*) as well as an inducible cyclooxygenase (COX-2) (*14*−*17*). Metabolically deficient mice have been used to demonstrate central roles for macrophage-derived reactive oxygen and nitrogen intermediates in host defense against pathogens (*18*, *19*). The prospect of radical coupling between $O_2^{\bullet-}$ formed in the NOX-catalyzed respiratory burst with $NO^{\bullet}$ from iNOS-catalyzed reactions to generate strongly oxidizing, but unstable peroxynitrite compounds (ONOOH and $ONOOCO_2^-$) (*20*) led to proposals (*21*−*25*) that peroxynitrite and/or secondary oxidizing radicals formed from it are important macrophage-generated toxins. This viewpoint has been disputed on the grounds that the expression of activities of NOX and NOS are temporally well separated events following macrophage activation and therefore that the peroxynitrite precursors $O_2^{\bullet-}$ and $NO^{\bullet}$ are never simultaneously present in significant quantities within the cell (*26*, *27*). Apparent peroxidase activity developing late in the life span of the activated cell has also been detected, which has alternatively been assigned to MPO activity (*26*, *27*) or peroxidase reactions involving COX-2 (*17*). In the present study, we have utilized a set of recently developed intracellular and extracellular chemical probes to more clearly define the nature and post-activation timing of oxidants generated by RAW 264.7 cells, which are often used as models for natural macrophages. On the basis of the data, we further suggest a new bactericidal mechanism operating in these cells, which is based upon the peroxidase-catalyzed formation of $NO_2^{\bullet}$ as the bacterial toxin (*28*).

EXPERIMENTAL PROCEDURES

Materials. Cultured murine-derived macrophages (RAW 264.7 ATCC #TIB-71 and CRL-2278) were grown in a water jacketed incubator under 5% CO_2 on a RPMI 1640 medium containing 300 mg/L L-glutamine and 5 mg/L phenol red (Invitrogen) supplemented with 50 mg/L gentamycin (Mediatech) and 10% fetal bovine serum (Invitrogen). Cells were grown to 90% confluence and were split 1:3 every 2 or 3 days to maintain healthy cultures. For experiments requiring cells in suspension, 90% confluent plates were harvested by using a cell scraper. The recovered cells were suspended in the reaction buffer, which was maintained on ice until the experiment was begun; cell densities were determined by counting an appropriately diluted sample on a hemocytometer in the presence of trypan blue.

2.7-Dichlorodihydrofluorescein (DCHF)-conjugated latex beads were prepared as follows: ~4.5×10^{10} amino-derivatized 1.0 μm polystyrene microspheres (Polysciences) were washed and suspended in 0.3 mL of 100 mM $NaHCO_3$ at pH 8.4, after which the suspension was purged with Ar and reacted with 10 mg of 2′,7′-dichlorodihydrofluorescein diacetate succinimidyl ester (Molecular Probes OxyBURST Green) dissolved in 1 mL of dry DMF. Following hydrolysis of the acetate protecting groups with hydroxylamine, the beads were washed in water and stored under Ar. This procedure gave beads with ~1.5×10^6 attached dichlorodihydrofluorescein molecules, as determined by comparison of the maximum fluorescence achieved from peroxynitrite-oxidized beads to authentic 2,7-dichlorofluorescein standards. Polyacrylamide microspheres were prepared by inverse microemulsion polymerization using a modified version of a published procedure (*29*). The emulsion was prepared by sonicating a two-phase system comprising 1 g of acrylamide, 250 mg of *N*,*N*′-methylenebisacrylamide, and 60 mg of potassium persulfate in 4 mL of H_2O and 1.2 g of 3:1 (w/w) Span 80 (sorbitan monooleate)/Tween-80 (polyethylene glycol-sorbitan monooleate) in 40 mL of hexane. Polymerization was initiated by adding 250 μL of *N*,*N*,*N*′,*N*′-tetramethylenediamine; after 10 min at room temperature, the particles that formed were recovered by centrifugation, washed sequentially with hexane and acetone, and dried overnight under vacuum, yielding 1.0 g of a white powder. A transmission electron microscopic analysis using a JEOL 100CX electron microscope indicated that the powder consisted of spherical microspheres with diameters ranging from 0.5 to 2.0 μm. The beads were digested in 0.5 M Na_2CO_3 at pH 10.5 for several hours at 85 °C to hydrolyze amide bonds, thereby generating carboxyl end groups (*30*). The modified beads were washed with water and acetone and dried overnight under vacuum; titration with standard HCl indicated the formation of ~8×10^8 carboxyl groups/bead. Fluorescein was then attached to the beads via a cystamine linker group using a previously described procedure that utilizes a carbodiimide coupling agent to form an amide bond between the cystamine and the bead carboxyl groups (*6*). The average number of attached dye molecules was ~4×10^7 per bead, as determined from the absorbance changes at 494 nm (ϵ_{494}(fluorescein) = 7.5×10^4 M^{-1} s^{-1}) when suspensions of beads were completely bleached with hypochlorous acid.

Reactions with Soluble Probes. For most experiments, the RAW cells were activated with 15 μg/mL of the endotoxin, *Escherichia coli* lipopolysaccharide (LPS) (Sigma), plus 20 U/mL of recombinant mouse IFγ (BD Biosciences). Alternatively, when just respiratory stimulation of the NADPH oxidase was desired, 200 ng/mL phorbol 12-myristate 13-acetate (PMA) (Sigma) was added to the medium. Two different activation procedures were used: in one, harvested cells were placed in 6-well plates and allowed to adhere overnight prior to adding the activators; in the other, the activators were simply added to the suspending buffer medium. Cell respiration rates were measured at 37 °C by continuously monitoring O_2 depletion in a thermostatted closed chamber containing a Clark-type polarographic electrode (Rank Bros.) whose output was connected to a stripchart recorder. For these experiments, the modified RPMI medium above the adherent cells was changed ~20 min before harvesting to bring the solution pH to 7.4 and restore nutrient levels. Following transfer of the harvested cells to the electrode chamber, the suspensions were briefly bubbled with O_2 from a syringe to adjust their concentrations to normal ambient conditions (0.2 atm). After an induction period of 5−10 min, O_2 uptake reached a steady rate that remained linear until the O_2 concentration fell below 0.1−0.05 atm. The chart recorder was calibrated by comparing the signal of air-saturated and anaerobic water, and the rate of O_2 consumption was determined from the linear portion of the trace, assuming that an air-saturated solution contained 0.25 mM O_2. Nitric oxide formation was measured as the accumulated levels of NO_2^- in the supernatant surrounding adherent cells by using the Griess assay (*31*). For these measurements, the standard culture medium was replaced by a medium devoid of phenol red (which interferes with

the colorimetric analysis). In these experiments, nitric oxide synthase (iNOS) involvement was probed by using 1 mM *N*-methyl-L-arginine (NMMA) as a competitive inhibitor of the enzyme. The acetate salt of NMMA (Sigma) was prepared as a 100 mM solution in HBSS. The Amplex Red assay (*32*) (Molecular Probes) was used to determine peroxide production by macrophages and the presence of a peroxidase within the cells. A 20 mM stock solution of the dye (10-acetyl-3,7-dihydroxyphenoxazine) was prepared in DMSO and stored at −20 °C. Horseradish peroxidase (HRP) stock solutions were prepared by dissolving HRP (Sigma) in 50 mM sodium phosphate at pH 7.4, to a concentration of 200 U/mL. The experiments were conducted on adherent cells in phosphate-buffered saline (PBS, 50 mM sodium phosphate at pH 7.4 plus 0.10 M NaCl) activated with LPS plus IFγ (LPS/IFγ). At desired times post-activation, 100 μM Amplex Red and 0.2 U/mL HRP were added to the supernatant and were allowed to incubate for 30 min for full color development. The supernatant was removed, and the intensity of the highly fluorescent product, resorufin (7-hydroxyphenoxazone), was spectrofluorimetrically determined by using a SPEX Fluorolog-3 instrument (λ_{ex}(max) = 527 nm; λ_{em}(max) = 595 nm). As a control, 300 μg/mL bovine liver catalase (Sigma) was added to scavenge H_2O_2. To analyze for peroxidase activity, HRP was omitted from the reaction medium. To analyze specifically for prostaglandin endoperoxide H synthase (COX) activity (*33*), adherent activated macrophages were harvested in reaction buffer and manually homogenized, after which 100 μM arachidonic acid (100 mM in methanol) (Sigma) and 50 μM Amplex Red were added to initiate the reaction. Two inhibitors were used in the COX analyses; 50 mM DuP-697 (Cayman), a COX-2 specific inhibitor, and 1 mM sodium azide, a general peroxidase inhibitor. Hydroethidine (HE), also known as dihydroethidium, was used to distinguish between the superoxide anion and other macrophage-generated oxidants (*34*). Stock solutions of 20 mM HE (Molecular Probes) were prepared in DMSO and stored protected from light at −20 °C. For these experiments, 50 μM HE was added to adherent activated cells in PBS at various times post-activation, then the cells were harvested, and changes in the fluorescence emission band of oxidized HE (λ_{ex} = 510 nm; λ_{em} = 540−750 nm) were subsequently monitored for ∼1.5 h. Catalase (300 μg/mL) and/or 100 U/mL bovine erythrocyte superoxide dismutase (SOD) (Sigma) were added to inhibit reactions of HE with extracellular H_2O_2 and $O_2^{\bullet-}$, respectively. Generation of $O_2^{\bullet-}$ and other one-electron oxidants was also probed by electron spin resonance (ESR) by using a series of cyclic hydroxylamines with differing lipophilicities (*35*−*37*), specifically, 1-hydroxy-4-phosphono-oxy-2,2,6,6-tetramethylpiperidine (PPH), 1-hydroxy-3-carboxy-2,2,5,5-tetramethylpyrrolidine (CPH), and 1-hydroxy-3-methoxycarbonyl-2,2,5,5-tetramethylpyrrolidine (CMH). The cyclic hydroxylamines (Alexis Biochemicals) were received as their hydrochloride salts; stock solutions were prepared by dissolving them in PBS to which 1 mM diethylenetriaminepentaacetic acid (DTPA) was added to inhibit metal ion-catalyzed hydroxylamine autoxidation. All stock solutions of the ESR probes were stored frozen at −20 °C. For ESR experiments, ∼1 × 10^5 macrophages/mL were harvested in PBS containing 200 μM DTPA and activated with PMA or LPS/IFγ. At designated times after activation, 0.5 mM of a hydroxylamine probe was added, and the suspension was transferred to a flat quartz cell mounted on a Bruker 300E ESR spectrometer; spectra were subsequently recorded at room temperature for ∼30 min. In some experiments, 300 μg/mL catalase and/or 100 U/mL SOD were added to inhibit extracellular reactions of the probes with H_2O_2 and $O_2^{\bullet-}$, respectively. Relative amounts of the nitroxide radicals formed were estimated from the peak-to-peak amplitudes of the low-field component of the triplet spectra. In both the HE fluorescence and ESR spin-trapping experiments, xanthine oxidase (XO)-catalyzed oxidation of xanthine was used as a standard source of $O_2^{\bullet-}$ and H_2O_2. Reagent concentrations for these reactions were 100 μM xanthine and 20 U/mL bovine milk XO (Calbiochem). Reactions with $NO^{\bullet}$ were investigated by bubbling anaerobic solutions of the probes with 99.5% $NO^{\bullet}$ from a compressed gas source (AGA Specialty Gas), which was purified by sequential passage through two scrubbing towers containing 2 M NaOH and one tower containing water. To minimize the introduction of adventitious O_2, all connecting lines consisted of glass tubing joined by greased 12/5 ball-and-socket joints. In some experiments, O_2 was deliberately added to the $NO^{\bullet}$ atmosphere to generate N_2O_3 and $NO_2^{\bullet}$. Reactions with $NO_2^{\bullet}$ were separately investigated by exposing N_2O-saturated solutions of the probes containing 1 mM KNO_2 to 1.1 krad/min γ-irradiation from a ^{60}Co source located at the Washington State University nuclear reactor facility (*28*, *38*); under these experimental conditions, this dose rate generates 9.5 μM $NO_2^{\bullet}$/min. The results from the various assays described above were normalized to the number of cells used in the experiment.

Intraphagosomal Reactions of Dye-Conjugated Particles. In these experiments, harvested macrophages were suspended at ∼1 × 10^7 cells/mL in phosphate buffer at pH 7.4 and challenged with a 20-fold excess of either DCHF-conjugated latex beads or opsonized fluorescein-conjugated polyacrylamide beads. Nearly equivalent results were obtained when the cells were activated with LPS/IFγ prior to mixing with the beads. Although the latex beads were readily phagocytosed without complement binding, uptake of the polyacrylamide beads was markedly facilitated by opsonization. This was accomplished by exposure to 25% fetal calf serum/75% Dulbecco's modified Eagle's medium (DMEM) for 30 min at 37 °C, followed by pelleting the beads and resuspending them in PBS. The suspensions were subsequently mixed at 37 °C by rotation on a Lab-Line multitube rotator. Small samples of the DCHF-conjugated bead/macrophage suspensions were periodically taken for fluorescence microscopic and spectrophotometric analyses of the oxidation of nonfluorescent DCHF to the highly fluorescent 2,7-dichlorofluorescein (DCF) product. Fluorescence microscopy allowed photographic analysis of the spatial location of oxidation and simultaneous fluorimetrically determined changes in fluorescence intensity allowed temporal monitoring of the extent of oxidation of the probe. For the latter measurements, the bead/cell suspensions were diluted 100-fold, and the emission spectrum from 515 to 580 nm was recorded under 495 nm excitation; for DCF, λ_{em}(max) = 523 nm.

Experiments utilizing the cystamine-linked fluorescein-polyacrylamide bead conjugate were undertaken to probe for certain oxidants (HOCl, $NO_2^{\bullet}$) that might be formed within the phagosome (*6*, *39*, *40*). At various times following phagocytosis, the dye was recovered by a process that

involved differential centrifugation of the suspension to isolate the cells from unphagocytosed beads, washing the pellet with water, manually homogenizing the cells, and treating the mixture with excess dithiothreitol (DTT) to cleave the disulfide bond of the linker group, thereby releasing the dye to the supernatant (*6*). The solubilized dye was then isolated by centrifugation to remove beads and cell debris, and its composition was analyzed by HPLC. For the analysis, 20 μL aliquots of the supernatant were run on a 5 μm reverse phase C-18 column using an isocratic mobile phase composed of 28% methanol and 72% 25 mM phosphate at pH 7.4. The column was mounted on a Gilson 305/306 HPLC instrument equipped for UV−visible absorbance detection, and chromatograms were determined at 495 nm, the visible absorption maximum of fluorescein. Quantitation of the signals was obtained with the use of authentic standards of the isolated fluorescein compound, monochloro and dichlorofluorescein derivatives prepared by reacting the fluorescein-conjugated beads with HOCl, and mononitro-derivatives prepared by reacting the conjugates with peroxynitrous acid in 25 mM bicarbonate buffers at pH 7.4 (*39*).

The fluorescein-conjugated polyacrylamide beads were also used to determine the intraphagosomal pH within the macrophage (*6*, *41*). The method used is based upon the intensity ratio of the fluorescein excitation bands at 437 and 491 nm, which are pH-sensitive over the range pH 4−9 (*42*). Calibration curves were constructed by suspending ~6 × 10^3 conjugated beads/mL in phosphate buffers with differing pH values and recording the excitation spectra at $\lambda_{em} = 510$ nm. Harvested macrophages were suspended to ~5 × 10^6 cells/mL in RPMI or RPMI plus 1 mM NaN_3 and challenged with ~2.5 × 10^6 opsonized beads. These suspensions were incubated at 37 °C under rotation; fluorescence microscopic analysis indicated that nearly all of the beads were phagocytosed within ~60 min after mixing. The mixture was periodically sampled by diluting 50 μL aliquots into 3 mL of PBS and immediately recording an excitation scan.

RESULTS

Selectivities of Probes for Various Oxidants. (*a*) *2,7-Dichlorodihydrofluorescein (DCHF)*. Exposure of DCHF-conjugated latex beads (0.05−5 × 10^8 beads/mL in PBS) to a saturating atmosphere of NO•, to ≤2 mM H_2O_2 in the absence of catalysts, or to a xanthine/XO catalytic system for generating $O_2^{\bullet-}$ and H_2O_2 for periods up to 40 min gave no perceptible oxidation to fluorescent products. However, controlled addition of air to the NO• atmosphere or addition of 0.2U/mL HRP or 300 μg/mL catalase to solutions containing H_2O_2 led to rapid and extensive oxidation of the dye to 2,7-dichlorofluorescein, as indicated by the fluorescence spectral maximum. Similarly, inclusion of catalase in the xanthine/XO assay promoted dye oxidation. The fluorescent oxidation product formed immediately upon exposure to ≤10 μM HOCl or <50 μM radiolytically generated $NO_2^{\bullet}$, and to oxidants generated in a standard Fenton system comprising 20 μM H_2O_2, 1.0 μM Cu^{2+}, and 1.0 mM ascorbate (*43*). Complete oxidation of DCHF on ~1 × 10^8 beads was attained upon bolus addition of 50 μM aliquots of peroxynitrite in either CO_2-free PBS or in 100 mM bicarbonate at pH 7.4, when the total added oxidant reached ~1 mM.

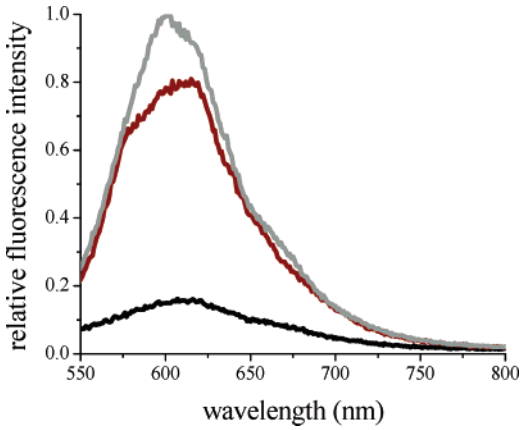

FIGURE 1: Reaction of HE with xanthine/XO-generated oxidants. Fluorescence spectra ($\lambda_{ex} = 510$ nm) after 5 min of incubation with 50 μM HE in PBS with 20 U/mL XO (black); XO plus 100 μM xanthine (gray); or XO/ xanthine plus 100 U/mL SOD (crimson). These data are representative of three experiments.

(*b*) *Hydroethidine (HE)*. The membrane-permeable dye, HE, has been shown to undergo oxidation by $O_2^{\bullet-}$ to give a unique fluorescent product, 2-hydroxyethidium (2-OH-E^+) (*44*), that is spectroscopically distinct from the fluorescent product, ethidium (E^+), formed by reaction with H_2O_2 and other biological oxidants (*34*). With the exception of this reaction, the pattern of oxidation of HE was qualitatively similar to that described above for DCHF. Specifically, oxidation of 50 μM HE in PBS with 2 mM H_2O_2 plus HRP, the H_2O_2/Cu^{2+}/ascorbate Fenton system, 250 μM HOCl, <50 μM $NO_2^{\bullet}$, 1 mM ONOOH or $ONOO^-/CO_2$, and 100 μM xanthine/(20U/mL) XO/(100 U/mL) SOD all gave spectroscopically indistinguishable fluorescent products with peak maxima at 615 nm, consistent with the formation of E^+ (*34*), whereas no appreciable reaction was observed when HE was exposed to ≤2 mM H_2O_2 either in the absence of catalysts or in the presence of 300 μg/mL catalase or to a saturating atmosphere of NO• for periods up to 30 min. As before, the introduction of O_2 into the NO• environment also gave rise to strong E^+ fluorescence. The $O_2^{\bullet-}$-generating xanthine/XO system, with or without 300 μg/mL catalase, gave a unique fluorescent product whose peak maximum was blue-shifted to 595 nm, consistent with the formation of 2-OH-E^+ (*44*). This signal persisted for at least 2 h. Representative spectra illustrating the formation of the two products in the xanthine/XO system are given in Figure 1. On the basis of these reactivity patterns, comparison of the onset and extent of fluorescence of HE and DCHF provides a means of identifying the role of respiration-generated $O_2^{\bullet-}$ in intracellular oxidant generation.

(*c*) *10-Acetyl-3,7-dihydroxyphenoxazine (Amplex Red)*. Reactions of 50 μM Amplex Red with the various oxidants closely followed the pattern exhibited by the DCHF-conjugated beads, with the exception that reaction with 100 μM HOCl gave no fluorescent product, and high dose levels of radiolytically generated $NO_2^{\bullet}$ (≤200 μM) were required to generate detectable fluorescence. This dye, which was used in the assays for peroxides and peroxidases, reacted rapidly with ONOOH or $ONOO^-/CO_2$, and H_2O_2/Cu^{2+}/ascorbate, H_2O_2/HRP, or H_2O_2/catalase, at the concentrations indicated above, as well as NO• plus O_2, to give intensely fluorescent solutions of resorufin that were several-hundred-fold greater than background levels but did not generate significant

Table 1: Reactivity Patterns of Oxidant Probes

	probe				
oxidant[a]	DCHF -beads	HE[b]	PPH	CPH/ CMH	Amplex Red
$O_2^{\bullet-}$	−	+	+	+	−
H_2O_2	−	−	−	−	−
H_2O_2/HRP	+	+	+	+	+
H_2O_2/cat	+	−	−	−	+
H_2O_2/Cu/asc	+	+	0	+	+
ONOOH	+	+	+	+	+
$ONOO^-/CO_2$	+	+	+	+	+
$NO^{\bullet}$	−	−	0	+	−
$NO_2^{\bullet}$	+	+	+	+	0
HOCl	+	+	+	+	−

[a] The reaction conditions for each oxidant are defined in the text. [b] Forms a unique spectroscopic product (2-OH-E^+) with $O_2^{\bullet-}$. The symbol 0 is meant to indicate the detection of a very minor reaction with nonphysiologically high concentrations of oxidant, and − indicates no detectable reaction.

amounts of fluorescent products when exposed to 100 μM HOCl, xanthine/XO-generated $O_2^{\bullet-}$, an anaerobic $NO^{\bullet}$ atmosphere, or 2 mM H_2O_2 in the absence of a peroxidase.

(*d*) *Cyclic Hydroxylamines (PPH, CPH, and CMH).* PBS solutions containing 50 μM of each cyclic hydroxylamine were exposed to the various oxidant systems described for the other probes, immediately after which their room-temperature ESR spectra were recorded. Comparisons of nitroxide signal peak intensities obtained under comparable reaction conditions indicated that for all oxidants examined, reactivities followed the order PPH < CMH < CPH. In general, xanthine/XO, HOCl, ONOOH, and $ONOO^-/CO_2$ under standard assay conditions and $NO_2^{\bullet}$ at dose levels as low as 10 μM all reacted strongly with the probes to give intense ESR signals. Strong signals were also observed upon reacting the Fenton system, H_2O_2/Cu^{2+}/ascorbate, with CMH and CPH or exposing anaerobic solutions of these probes to an atmosphere of $NO^{\bullet}$, but only very slight reaction was detected in either case with PPH. Hydrogen peroxide in the presence of DTPA was only marginally reactive toward each of the probes, confirming that the highly reactive oxidant in the xanthine/XO assay was $O_2^{\bullet-}$. This reactivity was only modestly increased (<3-fold) upon addition of HRP and was not increased upon addition of catalase to the assay medium.

The reactivity patterns observed for these probes in the various oxidant assays are shown in Table 1.

Respiratory Activation. Cells suspended in fresh RPMI media occasionally displayed a barely detectable increase in O_2 consumption above basal rates measured immediately after activation with LPS/IFγ; in individual experiments, the rate of this respiratory burst never exceeded 0.25 nmol O_2/10^6 cells-min, with an average value of 0.12 (±0.11) nmol $O_2/10^6$ cells-min. However, beginning at 2−4 h post-activation, respiration rapidly rose to a level of 1.5−2 nmol $O_2/10^6$ cells-min, which was ∼2 times the respiratory rate of unstimulated cells, 0.8 (±0.2) nmol $O_2/10^6$ cells-min. This enhanced rate was maintained over the subsequent lifetime of the cells (20−30 h). A major difference in the two cell lines was the onset time for enhanced respiration, which was ∼2 and ∼4 h post-activation for the CRL-2278 and TIB-71 cells, respectively. Representative results are shown in Figure 2.

Intracellular Generation of Oxidants. Phagocytosis of unopsonized DCFH-conjugated 1 μm latex beads by macrophages and the subsequent appearance of fluorescence in the cells were followed by fluorescence microscopy and spectroscopy as described in Experimental Procedures. At 30 min following mixing, many of the beads had adhered to the cells; phagocytosis leading to uptake of ∼80% of the beads occurred over the next ∼60 min, with each cell taking up 15−25 beads. By this point, fluorescence was not observed, indicating that oxidation of the dye was minimal (Figure 3). However, shortly thereafter, fluorescence from the entrapped beads rapidly increased (inset, Figure 4). This oxidation continued unabated at a steady rate over the entire 20 h of the experiment (Figure 4); this dynamic response was not appreciably altered by including 1 mM iNOS inhibitor, NMMA, or both NMMA and 300 μg/mL catalase in the reaction medium, or by omitting the soluble activators LPS and IFγ from the medium. However, stimulation with

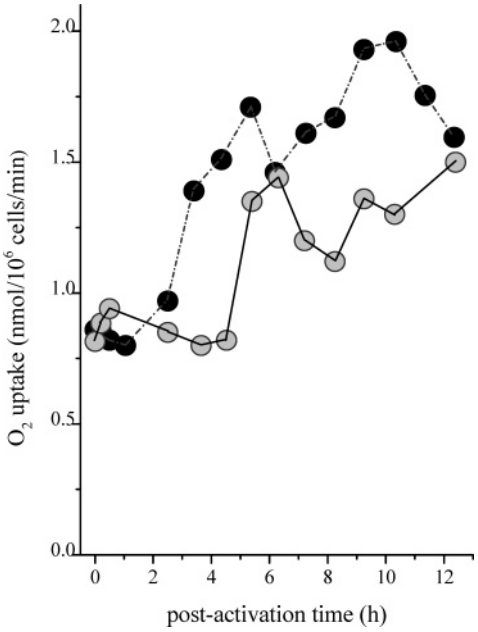

FIGURE 2: Respiration rates of LPS/IFγ-activated RAW cells. Gray and black circles represent data for TIB-71 and CRL-2278 cell lines, respectively. Cells were suspended in PBS at 37 °C immediately prior to measuring O_2 uptake. Data for each cell line are averages of two experiments. Very similar results were obtained when the measurements were extended to 25 h post-activation.

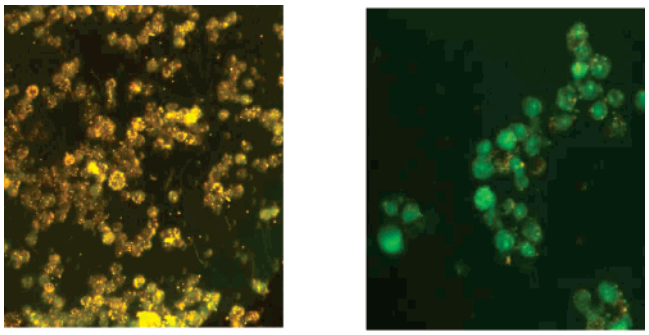

FIGURE 3: Phagocytosis of ∼2 × 10^8 DCHF-conjugated latex beads by ∼1 × 10^7 LPS/IFγ-activated TIB-71 cells. The photomicrograph labeled 2 h is scattered light taken before significant DCHF oxidation had occurred and displays the distribution of the beads and cells in suspension at that time. The photomicrograph labeled 8 h displays DCF fluorescence at 8 h post-phagocytosis, which occurs only from within the cells.

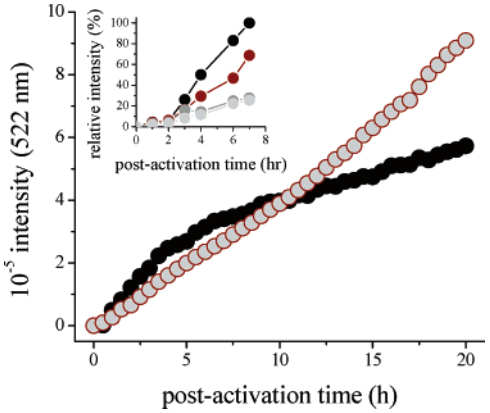

FIGURE 4: Oxidation of phagocytosed DCHF-conjugated latex beads by LPS/IFγ-activated RAW macrophages. ~1 × 10^7 TIB-71 (gray circles) or CRL-2278 cells (black circles) mixed with 2 × 10^9 beads at $t = 0$. Inset: initial changes following mixing of DCHF-beads with unactivated (crimson circles) or LPS/IFγ-activated (black circles) CRL-2278 cells, or with unactivated (light gray circles) or LPS/IFγ-activated (dark gray circles) TIB-71 cells. Spectra were recorded by scanning the emission from 515 to 580 nm with λ_{ex} = 495 nm. These data are representative of 5 experiments.

PMA appeared to elicit a greater rate of subsequent oxidation of the dye. The oxidative activity of CRL-2278 cells was generally greater than that of the TIB-71 cells at earlier times post-activation but then lagged somewhat after ~5 h (Figure 4). In several experiments, the suspensions of beads and cells were examined hourly with a fluorescence microscope; in these studies, the unphagocytosed fraction of DCHF-conjugated beads never acquired sufficient fluorescence over the 20 h duration of the experiment to become visually detectable (Figure 4), indicating that oxidation of the dye was limited primarily to beads located within the macrophage phagosome.

This conclusion is supported by comparisons of the extent of oxidation of the cyclic hydroxylamines, as determined by the intensities of EPR signals of the product nitroxides, which were an order of magnitude greater for the membrane-permeable probe, CMH, than for the less permeable CPH and impermeable PPH. This behavior is illustrated in Figure 5 for reactions with the probes at various times after activation of RAW cells with LPS/IFγ. Within 1 h post-activation, the RAW cells had acquired the capacity to oxidize CMH, which was maximized by 2.5 h and was retained over the life span of the activated cell. In contrast, the PPH cells underwent slightly increased oxidation at 1−2.5 h post-activation, but oxidation at subsequent times was negligible. Part of this difference is attributable to the greater reactivity of CMH noted above; however, the difference in reactivity between the two probes for the various oxidants under standard assay conditions was generally less than 3-fold. The much greater differences observed in oxidation levels for the two probes (Figure 5) is therefore consistent with the notion that the membrane-permeable probe (CMH) gained access to intracellular oxidants from which the membrane-impermeable probe (PPH) was excluded. The cyclic hydroxylamine, CPH, which is more reactive than PPH but also has limited membrane permeability under the experimental conditions (*35*, *36*), also formed considerably less nitroxide at the various times investigated.

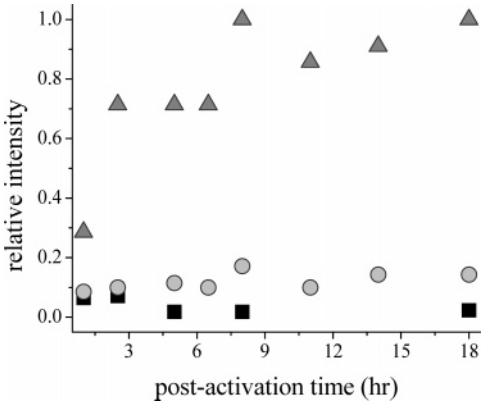

FIGURE 5: Nitroxide radical formation by reaction of the cyclic hydroxylamines, PPH (■), CPH (●), and CMH (▲) with LPS/IFγ-activated TIB-71 cells. The selected probe was added at a 0.5 mM concentration to ~1 × 10^5 cells/mL at the designated time after activation. ESR spectra were recorded in a flat quartz cell at 9.78 GH, 20 mW microwave power, 2 G modulation amplitude, and a time constant of 83 ms.

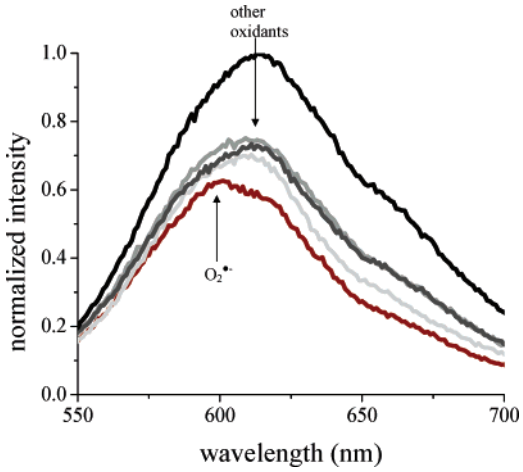

FIGURE 6: $O_2^{\bullet-}$ detection by HE in LPS/IFγ-activated TIB-71 cells. Fluorescence spectra obtained with λ_{ex} = 510 nm at 0.5 h (crimson), 1.5 h (light gray), 2.5 h (gray), 10 h (dark gray), and 20 h (black) after the addition of 50 μM HE to ~1 × 10^6 RAW macrophages. The arrows indicate the fluorescence spectral maxima observed in control studies using $O_2^{\bullet-}$ (595 nm) or the other oxidants (615 nm).

Formation of $O_2^{\bullet-}$. Despite the application of several different protocols, SOD-dependent ferricytochrome *c* reduction assays (*45*) gave no reproducible evidence of the formation of $O_2^{\bullet-}$ in PMA-stimulated or LPS/IFγ-activated RAW cells. However, when RAW cells were either stimulated with PMA or activated with LPS/IFγ in suspensions containing HE, a strong fluorescence signal developed over the following 30−90 min that contained the 595 nm band as the major component (Figure 6); this spectrum can be assigned to the product of the reaction of HE with $O_2^{\bullet-}$, that is, 2-OH-E^+ (Figure 1) (*44*). This reaction was not appreciably affected by the inclusion of SOD, SOD plus catalase, HRP, or sodium azide in the reaction medium, nor were significant differences found on this time scale between reactions of the two RAW cell variants. The addition of HE to either cell line at later times post-activation gave product spectra that exhibited no prominent feature at 595 nm but that showed a maximum at 615 nm, corresponding to the oxidized E^+ ion. The rate of oxidation based upon accumulated product was fairly constant to ~10 h post-

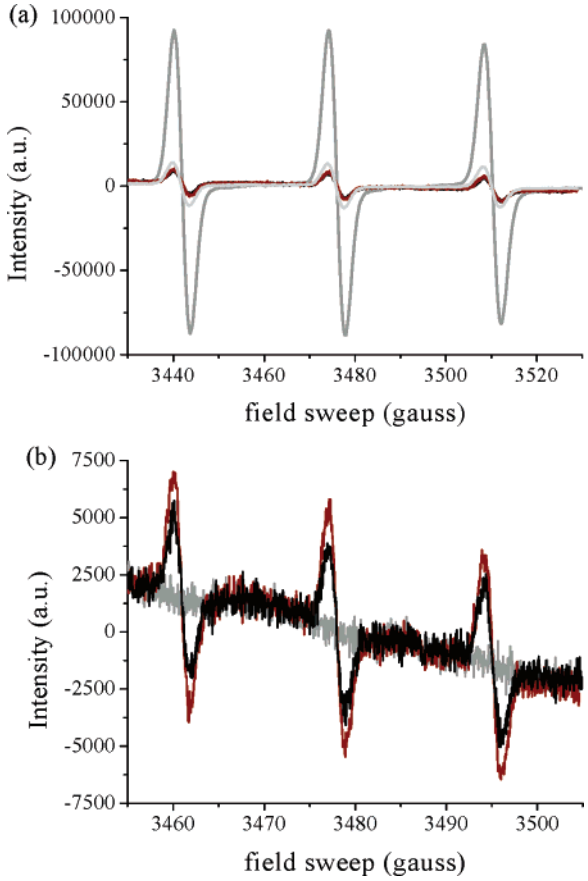

FIGURE 7: ESR spectra of the nitroxide 2,2,6,6-piperidinyloxyl, formed by one-electron oxidation of PPH. Panel a: 500 μM PPH alone (black), plus 100 μM xanthine (crimson), xanthine plus 20 U/mL xanthine oxidase (dark gray), or xanthine/XO plus 100 U/mL SOD (light gray). Panel b: 500 μM PPH plus $\sim 1 \times 10^5$ unactivated TIB-71 cells (gray) or 30 min after stimulating with 200 ng/mL PMA in the absence (crimson) or presence of 100U/mL SOD (black). ESR spectra were recorded in a flat cell under the conditions given in Figure 4, with the exception that the modulation amplitude was 1 G in panel a. The spectra shown in panel b are the averages of eight scans.

activation, but increased somewhat (20−30%) at later times (Figure 6).

Extracellular generation of $O_2^{\bullet-}$ was also probed by using the membrane-impermeable cyclic hydroxylamine, PPH. This compound undergoes one-electron oxidation by $O_2^{\bullet-}$ to the relatively stable 4-phosphonooxy-2,2,6,6,-tetramethyl-piperidinyloxy radical (PP$^\bullet$), which can be detected by ESR spectroscopy (*35*−*37*); as noted above, the H_2O_2 formed in the reaction is unreactive toward PPH, at least in the absence of enzyme catalysts. Addition of PPH to aerobic solutions containing xanthine/XO gave immediate formation of the characteristic 3-line ESR signal of PP$^\bullet$, which was quenched to background levels in the presence of SOD or SOD plus catalase (Figure 7a). Some oxidation of PPH was observed when the probe was added 30 min following stimulation of the cells with PMA (Figure 7b) or 1 h or 5 h following activation with LPS/IFγ; however, the same level of oxidation was observed in suspensions containing SOD, indicating that $O_2^{\bullet-}$ was not the oxidant.

Collectively, the data indicate that detectable amounts of $O_2^{\bullet-}$ form only within the cell and only within the first hour after stimulation or activation; in particular, the absence of influence of exogenous SOD or catalase on the reaction of

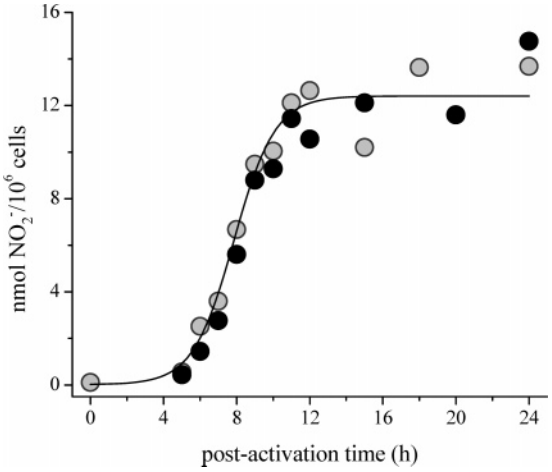

FIGURE 8: Accumulation of NO_2^- in media over LPS/IFγ-activated adherent RAW cells. Gray and black circles are data for TIB-71 and CRL-2278 cells, respectively. The solid line is a sigmoidal fit to the data, which are representative of seven experiments.

HE implies that intracellular reactions are being monitored, and the inability to detect $O_2^{\bullet-}$ by either ferricytochrome *c* or the more sensitive PPH assays implies that unlike granulocytes (*46*), very little exogenous $O_2^{\bullet-}$ is generated when the cells are stimulated with soluble agonists. From these data, we also infer that $O_2^{\bullet-}$ might contribute to CMH oxidation in activated RAW cells at the earliest time investigated ($\sim$0.5−1 h) (Figure 5) but that nitroxyl formation at subsequent times involves reaction with other intracellularly generated oxidants.

Formation of NO$^\bullet$. The concentration of NO_2^-, the stable catabolic end product of the reaction between NO$^\bullet$ and O_2, in the supernatant, increased dramatically at 4−10 h after activation of either cell line with LPS/IFγ and then underwent no further major change (Figure 8). The net rate of formation of NO$^\bullet$ was calculated from the first derivative of the accumulated yield of NO_2^- normalized to the amount of protein present; for individual runs, the calculated maximal rate of formation was 40−130 pmol $NO_2^-/10^6$ cells-min. Addition of the NOS inhibitor, NMMA, caused the amount of accumulated NO_2^- to decrease by >90%. When the cells were activated with just IFγ, accumulation of NO_2^- was markedly delayed and was detectable only at >15 h post-activation. Under these conditions, the subsequent rate of NO_2^- generation by the TIB-71 cells was $\sim$4-fold greater than that by the CRL-2278 cells.

Formation of Peroxides. Assays for peroxides in the media surrounding adherent cells was made using Amplex Red (*32*) with HRP as the catalyst. A small amount of peroxide formed within 1 h after PMA stimulation or LPS/IFγ activation, which subsequently declined several-fold over the next several hours (inset, Figure 9); because the formation and decay of this oxidant coincided with that of $O_2^{\bullet-}$, it is most likely H_2O_2 generated upon activation of the macrophage NADPH oxidase. At 5−8 h post-activation in both PMA- and LPS/IFγ-treated cells, the concentration level of HRP-reactive peroxides again rapidly increased, in this case to $\sim$10-fold the basal level, then underwent slow continued increase over the remainder of the 25−30 h lifetime of the cells (Figure 9). To better characterize the oxidant, the supernatant and cells were separated at various times post-activation and independently assayed for activity. The

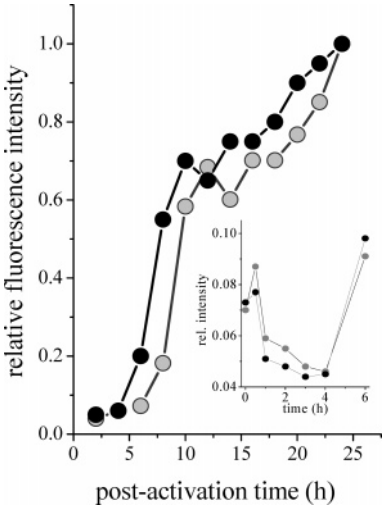

FIGURE 9: Accumulation of HRP-reactive peroxides in the extracellular medium of LPS/IFγ-activated RAW macrophages. The supernatant over $\sim 1 \times 10^6$ adherent cells was periodically sampled for reactive oxidants by adding Amplex Red and HRP and determining the resorufin yield. Inset: changes in HRP-reactive peroxides in media over TIB-71 (gray circles) and CRL-2278 (black circles) cells immediately following activation. Fluorescence spectra were scanned from 580 to 650 nm with $\lambda_{ex} = 527$ nm. These experiments were repeated five times with very similar results.

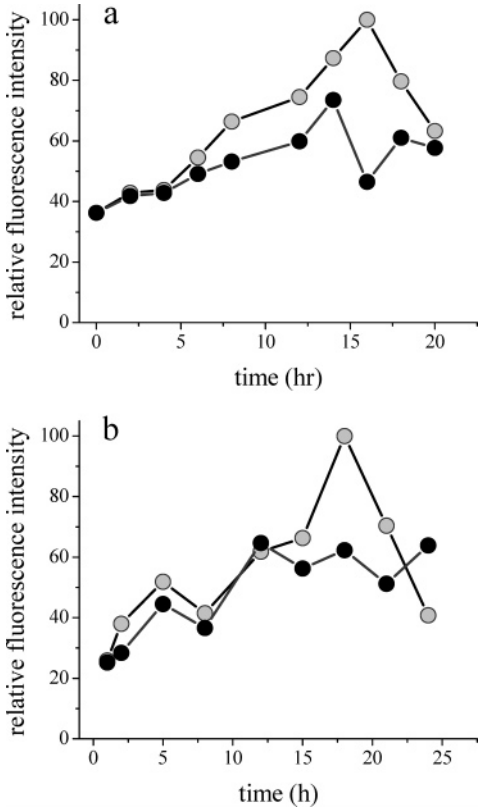

FIGURE 10: Cyclooxygenase (COX-2) activity in LPS/IFγ-activated TIB-71 cells. COX-2 activity was monitored by manual homogenization of $\sim 1 \times 10^6$ cells followed by additions of 50 μM Amplex Red and 100 μM arachidonic acid. Panel a: resorufin formation in the presence (black circles) and absence (gray circles) of 50 mM DuP-697. Panel b: resorufin formation in the presence (black circles) and absence (gray circles) of 1 mM N_3^-. Fluorescence spectra were scanned from 570 to 650 nm with $\lambda_{ex} = 527$ nm. These experiments were repeated three times with very similar results.

apparent rate of peroxide production by the cells in fresh buffer followed the trend shown in Figure 9, indicating that the peroxide concentration levels measured in the whole cell suspensions reflected the peroxide-generating activity of the cells. Similarly, the accumulated peroxide in the supernatant at various times coincided with the oxidant-generating activity of the cells. Unstimulated cells also produced HRP-reactive peroxides in amounts that coincided roughly with the basal levels measured at $\sim$2−3 h post-activation.

The supernatant was probed for the presence of an exogenous peroxidase by adding just Amplex Red to the reaction medium at 0−5 h post-activation. A small amount of resorufin was detected that corresponded to less than 10% of that formed in the standard HRP assay under comparable conditions. Furthermore, the fluorescence intensity did not increase with time in the manner that would be expected for an enzyme-catalyzed reaction, and the overall level of oxidation attained was constant over the investigated time interval. Consequently, any exogenous peroxidases that might exist in the cellular environment are below levels that are detectable with this sensitive assay.

Prostaglandin Endoperoxide H Synthase (COX) Activity. Induction of COX-2 cyclooxygenase activity was investigated by breaking the cells and assaying for resorufin formation with added arachidonic acid as substrate (*33*). A 2-fold enhancement of fluorescence was observed over background levels measured in the absence of arachidonate at 16−18 h post-activation in both cell lines; this arachidonate-dependent increase was not observed at other times following activation of the cells or when the COX-2-specific inhibitor, DuP-697, or the heme peroxidase inhibitor, N_3^-, was present in the medium (Figure 10). Thus, the inducible cyclooxygenase is implicated in the enhanced activity seen at 16−18 h, but not in the reaction at earlier times. The high background level of reactivity seen in these assays suggests the presence of a second arachidonate-dependent oxidative enzyme that is not inhibitable by N_3^-; lipoxygenases, for example, have these properties.

Intraphagosomal Alkalinization and Probes for Specific Oxidants. Cystamine-linked fluorescein−polyacrylamide bead conjugates have been used to detect chlorination within the phagosmes of neutrophils; specifically, fluorescence from the fluorescein reporter group of the phagocytosed probe underwent bathochromic shifts that are characteristic of ring chlorination and chemical analysis by HPLC and mass spectrometry of the recovered dye confirmed the formation of chlorofluorescein products (*6*). These fluorescein-conjugated beads also underwent facile ring nitration catalyzed by various peroxidases in media that contained NO_2^- and H_2O_2, although fluorescein nitration of the particulate probe was not detected within the neutrophil phagosome, even when phagocytosis was conducted in NO_2^--containing media (*39*). Two types of trapping experiments to probe for intraphagosomal nitration and chlorination reactions were undertaken in these studies. In one, the fluorescein-conjugated beads were mixed with activated RAW cells at various times (0, 2, 3, 6, 7, 8, 14, and 24 h post-activation), and the dye was recovered from the cellular milieu after 2 h of incubation by lysing the cells and cleaving the cystamine disulfide bond with dithiothreitol. In the other, phagocytosis of the particulate probes was used to activate the RAW cells, and the was dye subsequently recovered after incubation for

various time intervals extending to ~25 h post-phagocytosis. In neither case did the fluorescence spectra or HPLC chromatograms give any evidence of fluorescein chlorination or nitration.

Because fluorescein is not chemically modified following phagocytosis of the probe, the shape of the excitation band could be used to determine the intraphagosomal pH (*6*, *41*, *42*). Figure 11 shows the pH determined from the ratio of intensities at 437 and 491 nm based upon a calibration curve constructed from excitation spectra of the probes taken in buffered media. As is evident from the data, the intraphagosomal pH undergoes slow alkalinization from an initial value of ~6.5 to ~8.2 at 20 h post-phagocytosis. Inclusion of NaN_3 in the medium at a concentration that is sufficient to inhibit peroxidase activity (1 mM) had no effect upon the intraphagosomal pH changes.

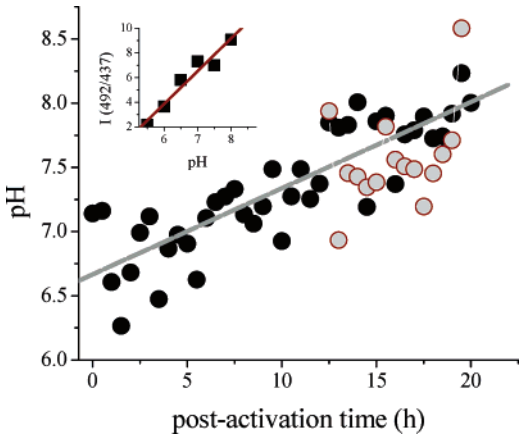

FIGURE 11: Intraphagosomal pH of TIB-71 cells determined with fluorescein-conjugated polyacrylamide microspheres. Excitation spectra from 400 to 500 nm were recorded at $\lambda_{em} = 510$ nm for suspension containing 5:1 bead/cell ratios. The gray circles are data points for media containing 1 mM N_3^-; the gray line is the best fit to the data obtained without N_3^-. Inset: calibration curve constructed from the fluorescence spectra of the beads in buffers at various pH values.

DISCUSSION

Reactivity Patterns of the Oxidant Probes. Each of the probes used to detect cellular oxidants was tested *in vitro* under a common set of conditions against 10 chemically or enzymatically generated oxidants; the qualitative results are summarized in Table 1. The standard conditions used for these tests were designed to expose the probes to greater amounts of each oxidant than would reasonably occur in the cellular milieu; consequently, the more significant entries are those that record absence of reaction with a particular oxidant. Viewed this way, the pattern observed for the DCHF-beads, for example, indicates that this probe is unreactive toward the primary products formed in reactions of the macrophage NADPH oxidase and nitric oxide synthases, that is, $O_2^{\bullet-}$, H_2O_2, and $NO^{\bullet}$, but is highly reactive toward all putative secondary oxidants that might be derived from them. Among the probes, only HE and the cyclic hydroxylamines reacted with $O_2^{\bullet-}$, and Amplex Red reacted efficiently only with H_2O_2/catalyst systems and the unstable peroxynitrite species. None of the probes reacted with the two-electron oxidant H_2O_2 in the absence of catalysts, and HE and the cyclic hydroxylamines were also unreactive during catalase-catalyzed H_2O_2 decomposition. Hypochlorous acid, also formally a two-electron oxidant (*47*), was reactive toward all of the probes except Amplex Red. All of the probes reacted with peroxynitrite-derived oxidants (*20*, *48*) and the Cu-catalyzed Fenton system (*43*), allowing no opportunity for discrimination among these species by reactivity pattern alone. Two of the cyclic hydroxylamines were oxidized in $NO^{\bullet}$-saturated solutions, but all other probes were unreactive.

The last reactions, that is, between $NO^{\bullet}$ and CPH or CMH to generate the corresponding nitroxides, are unexpected on thermodynamic grounds. A plausible reaction is net H-atom transfer yielding nitroxyl (HNO) and the stable nitroxide, that is, the reaction $R_2NOH + NO^{\bullet} \rightarrow R_2NO^{\bullet} + HNO$; however, estimates for the N-H bond energy in HNO and the O-H bond energy in R_2NOH are ~50 kcal/mol (Lymar, S. V., personal communication) and ~100 kcal/mol, respectively, making this reaction highly endergonic ($\Delta H \approx 50$ kcal/mol). One possible explanation is that the presence of excess $NO^{\bullet}$ causes rapid decomposition of HNO to N_2O and NO_2^- (*49*), thereby driving the hydroxylamine oxidation reaction forward, that is, the overall reaction is then $R_2NOH + 3NO^{\bullet} \rightarrow R_2NO^{\bullet} + N_2O + H^+ + NO_2^-$. This reaction would not be expected to occur under physiological conditions, however, where transient concentration levels of $NO^{\bullet}$ are orders of magnitude lower than under the imposed *in vitro* reaction conditions. Consequently, CPH and CMH are probably also unreactive toward biologically generated $NO^{\bullet}$.

Oxidant Generation by Activated RAW 264.7 Cells. (*a*) *Topographic Location*. The response of the probes used in these studies to RAW cells was independent of the activation method. Thus, the post-activation time course and apparent levels of oxidation appeared indistinguishable when cells were activated by PMA, the dye-conjugated particles, or LPS/IFγ. As described in the Results section, oxidant generation was largely intracellular, as indicated by the spatial location of fluorescence from the oxidized DCHF-latex beads (Figure 4) and the differential reactivities observed for the membrane-impermeable (PPH) and membrane-permeable (CMH) ESR probes (Figure 5). This intracellular localization makes it difficult to determine effective concentrations of various reactive species generated by the cells.

(*b*) *Superoxide Generation.* Immediately following activation, $O_2^{\bullet-}$ formation was observed by its reaction with the membrane-permeable dye, HE, to give the spectroscopically unique oxidation product, 2-OH-E^+ (Figure 6); at times longer than ~1 h, this product was no longer detectable, although reactions with other cellularly generated oxidants to form E^+ occurred over the entire life span of the activated cell. The absence of appreciable reaction with PPH indicated that release of $O_2^{\bullet-}$ into the extracellular medium was negligible under all conditions. This behavior contrasts markedly with neutrophils, which, in the 30−60 min interval following stimulation with PMA and other soluble agonists, generate readily detectable $O_2^{\bullet-}$ the extracellular medium in reactions catalyzed by their plasma membrane-localized NADPH oxidase (*46*, *50*). Stimulation of neutrophils with PMA gives extracellular generation of $O_2^{\bullet-}$ at optimal rates which are typically 2−3 nmol $O_2^{\bullet-}/10^6$ cells-min (*46*), whereas the highest rate reported for PMA-stimulated macrophages has been 0.5 nmol $O_2^{\bullet-}/10^6$ cells-min, measured for isolated rat alveolar cells (*21*). However, much lower

values have been measured for LPS/IFγ-activated RAW 264.7 cells (*26*) and mouse peritoneal macrophages (*27*). The very limited amounts of $O_2^{\bullet-}$ detected in these assays are in accord with our findings using HE and cyclic hydroxylamines as $O_2^{\bullet-}$ trapping agents (Figures 6 and 7) and with the vanishingly small respiratory simulation measured immediately following activation (Figure 2), which implies very low NOX activity in the activated RAW cells. The average net respiratory increase in RAW cells of 0.12 nmol $O_2/10^6$ cells-min can be compared to an optimal value of ~5 nmol $O_2/10^6$ cells-min for PMA-stimulated human neutrophils (*6*).

(*c*) *Nitric Oxide Generation.* The existence of an inducible nitric oxide synthase within macrophages was suggested 20 years ago when it was shown that LPS from *E. coli* induced the biosynthesis of NO_2^- and NO_3^- in mouse macrophages (*12*, *13*). Accumulation of these ions was enhanced in the presence of T-lymphocytes, which release inflammatory cytokines during the immune response, or by direct addition of the cell-free cytokines themselves. In these studies, the ions accumulated rapidly during the first 16 h post-activation with LPS and IFγ, after which the rate of accumulation slowed over the next 32 h (*51*). Because NO_2^- and NO_3^- have been identified as catabolic end products of $NO^\bullet$, they have been used widely as indicators of NOS activity. More recently, direct electrochemical detection of $NO^\bullet$ in Mayer's laboratory has confirmed these assumptions (*26, 27*). In particular, it was shown that $NO^\bullet$ production within the supernatant of LPS/IFγ-treated RAW 264.7 cells occurred primarily at 5−10 h post-activation with the formation rate peaking at ~8 h and that this activity was paralleled by NO_2^- accumulation in the medium. Very similar timing has also been reported by Ullrich and co-workers (*17*), and our results (Figure 8) are fully in accord with these observations. Because the formation of each NO_2^- from arginine in NOS-catalyzed reactions requires 2.0−2.25 O_2 molecules (*52*) (depending upon the mechanism of oxidation of $NO^\bullet$), the rate of O_2 consumption corresponding to the maximal rate of NO_2^- accumulation (~ 80 pmol/10^6 cells-min) is 160−180 pmol/10^6 cells-min. The corresponding respiration rate at ~8 h post-activation is ~1.5 nmol/10^6 cells-min so that at any time, ≤15% of the overall O_2 consumption by the cells is directed at the generation of reactive nitrogen species, and at most, ~25% of the increased respiration over the basal level of resting cells can be attributed to these reactions.

(*d*) *Prospects for Peroxynitrite Formation*. In the absence of evidence to the contrary, it has historically been assumed that the macrophage NOX is similar to that found in neutrophils. However, a major difference now appears to be the extent of respiratory activation upon agonist stimulation. Activated macrophages, through their capacity to generate both $O_2^{\bullet-}$ and $NO^\bullet$, are often presumed to be a biological source of ONOOH and $ONOO^-/CO_2$ (*21*−*25*, *53*). However, as has been emphasized by Mayer and associates (*26*, *27*) and reinforced by these studies, there is very little temporal overlap in the formation of these radicals, at least in RAW cells, which should preclude significant formation of peroxynitrite by a radical coupling mechanism. Additionally, the exceedingly low amounts of $O_2^{\bullet-}$ formed in the RAW cells, approaching the detectable limits of sensitive trapping methods, sets a very low stoichiometric limit on the amount of peroxynitrite that could possibly be generated by them. Nitration of phenolic compounds, including protein tyrosyl groups, has been cited as evidence consistent with peroxynitrite generation in macrophages (*21, 23*). Although nitro-substituted compounds are readily formed from peroxynitrite-derived oxidants (*20*, *40*), their formation in biological environments is not diagnoistic for peroxynitrite; other potential biological nitrating agents include reactive nitrogen intermediates formed during $NO^\bullet$ autoxidation and in peroxidase-catalyzed oxidation of NO_2^- (*54*). Mayer and co-workers have reported that 3-nitrotyrosine accumulates at 15−25 h post-activation in RAW cells (*26*) and appears at about the same time in peritoneal macrophages (*27*). This timing is far too late to involve NOX-generated $O_2^{\bullet-}$ and was suggested to involve nitrite-dependent peroxidase catalyzed reactions. On the basis of these considerations, the likelihood of significant peroxynitrite formation via simultaneous generation of $O_2^{\bullet-}$ and $NO^\bullet$ appears remote.

If the phagosome underwent substantial acidification, the reaction of cellularly generated H_2O_2 with accumulated NO_2^- to give ONOOH could occur (*55*); however, use of fluorescein-conjugated polyacrylamide beads has indicated only a steady progressive alkalinization of the cells following phagocytosis (Figure 11), precluding this reaction. This latter result is itself surprising, as previous studies had indicated that the phagosomes of mouse peritoneal macrophages challenged with fluorescein-conjugated *Staphylococcus aureus* underwent rapid acidification to pH ~6 (*56, 57*); this acidification was driven by the electrogenic transport of protons via a V-type H^+-ATPase.

(*e*) *Cyclooxygenase Activity*. An inducible prostaglandin endoperoxide H synthase (COX-2) was shown to be present in LPS/IFγ-activated RAW 264.7 cells a decade ago by experiments that measured rates of conversion of arachidonic acid to the prostaglandin PGE_2 and antibody-specific accumulation of enzyme in isolated microsomal fractions, as well as expression of COX-2 mRNA (*14*); earlier studies had established that LPS also induced cyclooxygenase activity in alveolar macrophages and monocytes (*58*−*60*). This activity was maximal in the RAW cells ~24 h post-activation, although the corresponding mRNA expression was maximal at ~8 h post-activation (*14*). The Amplex Red assay has been adapted to COX reactions by using arachidonic acid as substrate (*32*); by using the COX-2 specific inhibitor (Dup 697) in disrupted cells, we have identified its presence over a time range of ~10−20 h post-activation in both of the investigated cell lines (Figure 10); this induction time is very similar to recently published results obtained with LPS-activated RAW cells (*17*) and another immortalized murine macrophage (J774.2) activated with LPS/IFγ (*16*).

(*f*) *Other Oxidase/Oxygenase/Peroxidase Activities.* The increased rates of O_2 consumption beginning at several hours post-activation (Figure 2) could arise either from respiratory uncoupling in the mitochondria or activation of other oxidase and/or oxygenase pathways. In either case, as discussed below, these reactions lead to increased oxidizing capacity within the cell. These rate increases cannot be attributed solely to iNOS activation or to iNOS plus COX-2 activation because the stimulated O_2 uptake precedes the induction of activities of these enzymes (cf. Figures 2, 8 and 10; this temporal separation between respiratory stimulation and iNOS activation is most evident for the CRL-2278 cells).

Furthermore, as previously noted, the amount of $NO^{\bullet}$ detected as NO_2^- was only a small fraction of the consumed O_2.

The increased oxidizing capabilities of the cells was most evident in the oxidation of the phagocytosed DCHF-latex beads, which was detected ~2 h following phagocytosis and continued over the entire life span of the cells (Figure 4). In these studies, the onset and initial rates of increase in fluorescence intensities in the CRL-2278 RAW cells preceded those of TIB-71 cells (Figure 4, inset), paralleling the respiratory behavior (Figure 2). Oxidation of CMH to its EPR-detectable nitroxide was also observed on this time scale (Figure 5); although some of the nitroxide formation might be attributable to reaction with $O_2^{\bullet-}$, it is clear that most of the oxidizing capacity of the cells developed after ~1 h, at which time the $O_2^{\bullet-}$-generating capacity of the cells was no longer detectable (Figure 6). In any event, intracellular oxidation of DCHF clearly indicates the presence of an alternate oxidant because the dye is unreactive toward $O_2^{\bullet-}$ (Table 1). Likewise, these reactions cannot be attributed simply to accumulation of NOX-generated H_2O_2 because DCHF and CMH, although relatively indiscriminant (Table 1), are both unreactive toward H_2O_2.

An HRP-reactive oxidant appeared in the extracellular medium and increased over the same time period (5−10 h), and was then maintained over the ensuing lifetime of the cell (Figure 9). One notes again that the induction time for detection of this oxidant was ~2 h shorter for the CRL-2278 cells, consistent with its generation by induced O_2-consuming enzymatic systems other than iNOS and COX-2. This oxidant was stable, as was established by separating the supernatant medium from the cells prior to applying the Amplex Red/HRP assay; this demonstration excludes the possibility that the oxidant was $NO_2^{\bullet}$ or peroxynitrite-derived oxidants, which are very short-lived under the experimental conditions ($t_{1/2}$ < 10 s) (*20*, *48*, *61*). The oxidant is most likely H_2O_2, given its membrane permeability (*62*, *63*) and the high selectivity (*64*) of HRP for this peroxide. Addition of Amplex Red without HRP to the medium and/or to adherent cells gave negligible reaction, indicating that the cells were not excreting an extracellular peroxidase. Hypochlorous acid, because it is unreactive in the Amplex Red assay (Table 1), is clearly not the oxidant.

The reactivity characteristics of DCHF and CMH allow further delineation of the induced enzyme systems involved in the oxidative reactions, which could be either oxygenases or peroxidases. Catalase involvement can be excluded, at least for CMH oxidation, because the cyclic hydroxylamine is unreactive toward H_2O_2/catalase (Table 1). Mayer and co-workers have proposed that myeloperoxidase (MPO), by catalyzing the one-electron oxidation of NO_2^- to $NO_2^{\bullet}$, is responsible for the 3-nitrotyrosine formation detected within RAW cells following iNOS expression. In support of this proposal, these researchers also demonstrated by selective immunoblotting the presence of low levels of MPO within the cell (*26*); however, the amount of MPO did not change perceptibly upon activation of the cells. From our perspective, it seems unlikely on three counts that MPO is the intracellular oxidation catalyst. First, both DCHF and CMH are reactive toward HOCl and in peroxidase-catalyzed reactions with H_2O_2 (Table 1); if MPO were the peroxidase, then conditions existing immediately following NOX activation in PBS should have caused some probe oxidation, but none was detected in this time frame (Figure 4). Second, MPO is ineffective within phagosomes at nitrating phenolic compounds, the dominant reaction being ring chlorination under physiological conditions (*39*). Third, attempts to trap intracellular MPO-generated HOCl by using fluorescein-conjugated phagocytosable polyacrylamide beads (*6*) gave negative results under widely varying experimental protocols, indicating that the expression of MPO activity within the cells must be very low. In particular, during the oxidative period prior to iNOS activation, probe chlorination should have been readily detected were MPO a major contributor to the oxidative reactions. Alternatively, the substrate and inhibitor specificities (*65*) associated with the high background activity (~50%) suggest the participation of an active lipoxygenase (LOX) in the intracellular generation of reactive oxygen species (ROS). A precedent for this behavior can be found in mammalian mast cells, which have recently been shown by inhibition studies to generate internal DCHF-reactive compounds following IFγ stimulation that are LOX dependent but independent of NOX or NOS expression (*66*−*68*). Although the underlying redox chemistry remains to be established, these studies demonstrate that reactive species other than $NO_2^{\bullet}$ are generated by activated RAW cells because the Amplex Red assay is insensitive to this radical (Table 1).

Physiological Implications. In the absence of significant MPO activity and limited capacity to form peroxynitrite, the only recognized microbicidal mechanisms available to these cells involve metal-mediated Fenton reactions (*43*, *69*). However, Ullrich and co-workers have presented data indicating that inhibition of COX-2 activity within LPS-stimulated RAW cells correlates with nitration of some of its own tyrosyl groups; the inhibitory reaction was arachidonate- and NO_2^--dependent and could not be catalyzed by MPO or catalase in *ex vivo* assays, the inference being that it is autocatalytic (*17*). This reaction was detected at 12−16 h post-activation, at which time NO_2^- accumulation was optimal ((*17*), Figure 4). Furthermore, as noted above, Mayer and co-workers have reported widespread tyrosyl nitration within LPS/IFγ-activated RAW cells within roughly the same time scale (*26*); although in this case the target sites were not identified, they must have involved other intracellular proteins. These data suggest that like all other heme peroxidases that have been investigated (*39*, *70*), COX-2 can oxidize available NO_2^- at its peroxidase site (*71*) via peroxide-generated compounds I and II to $NO_2^{\bullet}$, which is then diffusible from the active site. We recently found that $NO_2^{\bullet}$ is remarkably toxic to *Escherichia coli*, with an LD_{50} comparable to that of the much more strongly oxidizing and potently microbicidal $CO_3^{\bullet-}$ radical anion (*28*), and Klebanoff has demonstrated that *E. coli* are also effectively killed when exposed to a cell-free MPO−H_2O_2−NO_2^- system (*70*). Sequential induction of LOX, iNOS, and COX-2 could lead to the development of bactericidal potential within the cell by arginine and lipid autoxidation to generate $NO_2^{\bullet}$ in the manner suggested in Scheme 1. In this hypothetical scheme, (1) LOX functions to generate lipid hydroperoxides from reaction of O_2 with endogenous lipids (*72*) for (2) activation of and use by COX-2 (*71*) in reactions with NO_2^- (3) formed by iNOS-catalyzed arginine oxidation by O_2 (*52*) and subsequent aerobic oxidation of $NO^{\bullet}$ (*61*). Recent studies have revealed a complex interaction between iNOS and

Scheme 1: Hypothetical Mechanism for the Induction of Microbicidal Potential in RAW 264.7 Cells[a]

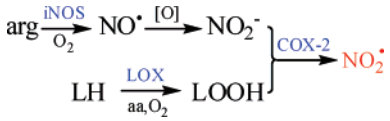

[a] aa = arachidonic acid.

COX-2, which may involve physical association of the two enzymes (*73*), COX-2 catalyzed consumption of NO• (*16*), modification of COX-2 activity via S-nitrosylation (*73*), and possibly inactivation of COX-2 by radical coupling of its essential tyrosyl radical with iNOS-generated NO• (*74*). Inhibition of NO_2^- accumulation at ~12 h post-activation (Figure 8) may be one manifestation of these interactions, that is, expression of COX-2 activity diverts NO• consumption to other products. In any event, the observed timing of events (iNOS > COX-2) would allow elevation of NO_2^- levels within the cell for use as a COX-2 substrate.

ACKNOWLEDGMENT

We are indebted to Jonathan Cape at the WSU EPR Center for assistance in conducting studies on the oxidation of cyclic hydroxylamines, to Dr. Linyong Zhu for synthesizing fluorescein-conjugated polyacrylamide beads and Kristen Kelson for undertaking phagocytosis studies with them, to David King for assistance in acquiring the radiolysis data reported herein, and to Sergei Lymar at Brookhaven National Laboratory for helpful discussions concerning reactions between NO• and hydroxylamines.

REFERENCES

1. Tauber, A. I., and Chernyak, L. (1991) *Metchnikoff and the Origins of Immunology. From Metaphor to Theory*, Oxford University Press, New York.
2. Klebanoff, S. J., and Clark, R. A. (1978) *The Neutrophil—Function and Clinical Disorders*, North-Holland, Amsterdam, The Netherlands.
3. Klebanoff, S. J. (1988) Phagocytic Cells: Products of Oxygen Metabolism, in *Inflammation: Basic Principles and Chemical Correlates* (Gallin, J. I., Goldstein, I. M., and Snyderman, R., Eds.) pp 391−444, Raven Press, New York.
4. Kettle, A. J., and Winterbourn, C. C. (1997) Myeloperoxidase: a key regulator of neutrophil oxidant injury, *Redox Rep. 3*, 3−15.
5. Hampton, M. B., Kettle, A. J., and Winterbourn, C. C. (1996) Involvement of superoxide and myeloperoxidase in oxygen-dependent killing of *Staphylococcus aureus* by neutrophils, *Infect. Immun. 64*, 3512−3517.
6. Jiang, Q., Griffin, D. A., Barofsky, D. A., and Hurst, J. K. (1997) Intraphagosomal chlorination dynamics and yields determined using unique fluorescent bacterial mimics, *Chem. Res. Toxicol. 10*, 1080−1089.
7. Chapman, A. L. P., Hampton, M. B., Senthilmohan, R., Winterbourn, C. C., and Kettle, A. J. (2002) Chlorination of bacterial and neutrophil proteins during phagocytosis and killing of *Staphylococcus aureus*, *J. Biol. Chem. 277*, 9757−9762.
8. Rosen, H., Crowley, J. R., and Heinecke, J. W. (2002) Human neutrophils use the myeloperoxidase-hydrogen peroxide-chloride system to chlorinate but not nitrate bacterial proteins during phagocytosis, *J. Biol. Chem. 277*, 30463−30468.
9. Segal, A. W. (2005) How neutrophils kill microbes, *Annu. Rev. Immunol. 23*, 197−223.
10. Ding, A. H., and Nathan, C. F. (1987) Trace levels of bacterial lipopolysaccharide prevent interferon-γ or tumor necrosis factor-α from enhaning mouse peritoneal respiratory burst capacity, *J. Immunol. 39*, 1971−1977.
11. Forman, H. J., and Torres, M. (2002) Reactive oxygen species and cell signaling. Respiratory burst in macrophage signaling, *Am. J. Respir. Crit. Care Med. 166*, 54−58.
12. Stuehr, D. J., and Marletta, M. A. (1985) Mammalian nitrate biosynthesis: mouse macrophages produce nitrite and nitrate in response to *Escherichia coli* lipopolysaccharide, *Proc. Natl. Acad. Sci. U.S.A. 82*, 7738−7742.
13. Stuehr, D. J., and Marletta, M. A. (1987) Induction of nitrite/nitrate synthesis in murine macrophages by BCG infection, lymphokines, or interferon-γ, *J. Immunol. 139*, 518−525.
14. Riese, J., Hoff, T., Nordhoff, A., DeWitt, D. L., Resch, K., and Kaever, V. (1994) Transient expression of prostaglandin endoperoxide synthase-2 during mouse macrophage activation, *J. Leukocyte Biol. 55*, 476−482.
15. Jang, B.-C., Kim, K.-H., Park, J.-W., Kwon, T. K., Kim, S.-P., Song, D.-K., Park, J.-G., Bae, J.-H., Mun, K.-C., Bake, W.-K., Suh, M.-H., Hla, T., and Suh, S.-I. (2004) Induction of cyclooxygenase-2 in macrophages by catalase: role of NF-κB and PI3K signaling pathways, *Biochem. Biophys. Res. Commun. 316*, 398−406.
16. Clark, S. R., Anning, P. B., Coffey, M. J., Roberts, A. G., Marnett, L. J., and O'Donnell, V. B. (2005) Depletion of iNOS-derived nitric oxide by prostaglandin H synthase-2 in inflammation-activated J774.2 macrophages through lipohydroperoxidase turnover, *Biochem. J. 385*, 815−821.
17. Schildknecht, S., Heinz, K., Daiber, A., Hamacher, J., Kavaklí, C., Ullrich, V., and Bachschmid, M. (2006) Autocatalytic tyrosine nitration of prostaglandin endoperoxidase synthetase-2 in LPS-stimulated RAW 264.7 macrophages, *Biochem. Biophys. Res. Commun. 340*, 318−325.
18. Shiloh, M. U., MacMicking, J. D., Nicholson, S., Brause, J. E., Potter, S, Marino, M., Fang, F., Dinauer, M., and Nathan, C. (1999) Phenotype of mice and macrophages deficient in both phagocyte oxidase and inducible nitric oxide synthase, *Immunity 10*, 29−38.
19. Murray, H. W., and Nathan, C. F. (1999) Macrophage microbicidal mechanisms in vivo: reactive nitrogen versus oxygen intermediates in the killing of intracellular visceral *Leishmania donovani*, *J. Exp. Med. 189*, 741−746.
20. Goldstein, S., Lind, J., and Merényi, G. (2005) Chemistry of peroxynitrites as opposed to peroxynitrates, *Chem. Rev. 105*, 2457−2470.
21. Ischiropoulos, H., Zhu, L., and Beckman, J. S. (1992) Peroxynitrite formation from macrophage-derived nitric oxide, *Arch. Biochem. Biophys. 298*, 446−451.
22. Li, H., Hu, J., Xin, W., and Zhao, B. (2000) Production and interaction of oxygen and nitric oxide free radicals in PMA stimulated macrophages during the respiratory burst, *Redox Rep. 5*, 353−358.
23. Linares, E., Giorgio, S., Mortara, R. A., Santos, C. X. C., Yamada, A. T., and Augusto, O. (2001) Role of peroxynitrite in macrophage microbicidal mechanisms in vivo revealed by protein nitration and hydroxylation, *Free Radical Biol. Med. 30*, 1234−1242.
24. Juliet, P. A. R., Hayashi, T., Iguchi, A., and Ignarro, L. J. (2003) Concomitant production of nitric oxide and superoxide in human macrophages, *Biochem. Biophys. Res. Commun. 310*, 367−370.
25. Alvarez, M. N., Piacenza, L., Irigoin, F., Peluffo, G., and Radi, R. (2004) Macrophage-derived peroxynitrite diffusion and toxicity to *Trypanosoma cruzi*, *Arch. Biochem. Biophys. 432*, 222−232.
26. Pfeiffer, S., Lass, A., Schmidt, K., and Mayer, B. (2001) Protein tyrosine nitration in cytokine-activated murine macrophages, *J. Biol. Chem. 276*, 34051−34058.
27. Pfeiffer, S., Lass, A., Schmidt, K., and Mayer, B. (2001) Protein tyrosine nitration in mouse peritoneal macrophages activated in vitro and in vivo: evidence against an essential role of peroxynitrite, *FASEB J. 15*, 2355−2364.
28. King, D. A., Sheafor, M. W., and Hurst, J. K. (2006) Comparative toxicities of putative phagocyte-generated oxidizing radicals toward a bacterium (*Escherichia coli*) and a yeast (*Saccharomyces cerevisiae*), *Free Radical Biol. Med. 41*, 765−774.
29. Goh, S. A., Murthy, N., Xu, M., and Fréchet, J. M. J. (2004) Cross-linked microparticles as carriers for the delivery of plasmid DNA for vaccine development, *Bioconjugate Chem. 15*, 467−474.
30. Inman, J. K. (1974) Covalent linkage of functional groups, ligands and proteins to polyacrylamide beads, *Methods Enzymol. 34*, 31−58.
31. Greenbert, A. E., Conners, and J. J., Jenkins, D. (1995) *Standard Methods for the Examination of Water and Wastewater*, 15th ed., pp 4−99, American Public Health Association, United Book Press, Baltimore, MD.
32. Zhou, M., Diwu, Z., Panchuk-Voloshina, N., and Haugland, R. P. (1997) A stable nonfluorescent derivative of resorufin for the

fluorometric determination of trace hydrogen peroxide: application in detecting the activity of phagocyte NADPH oxidase and other oxidases, *Anal. Biochem. 253*, 162−168.
33. Batchelor, R., Johnson, I., and Beechem, J. (2003) A Fluorometric Assay for Cyclooxygenase Enzymes, Annual Meeting of the Society for Biomolecular Screening, Portland, OR.
34. Zhao, H., Kalivendi, S., Zhang, H., Joseph, J., Nithipatikom, K., Vásquez-Vivar, J, and Kalyanaraman, B. (2003) Superoxide reacts with hydroethidine but forms a fluorescent product that is distinctly different from ethidium: potential implications in intracellular fluorescence detection of superoxide. *Free Radical Biol. Med. 34*, 1359−1368.
35. Dikalov, S., Grigor'ev, I. A., Voinov, M., and Bassenge, E. (1998) Detection of superoxide radicals and peroxynitrite by 1-hydroxy-4-phsphonooxy-2,2,6,6,-tetramethylpiperidine, *Biochem. Biophys. Res. Commun. 248*, 211−215.
36. Fink, B., Dikalov, S., and Bassenge, E. (2000) A new approach for extracellular spin trapping of nitroglycerin-induced superoxide radicals both in vitro and in vivo, *Free Radical Biol. Med. 28*, 121−128.
37. Dikalov, S. I., Dikalova, A. E., and Mason, R. P. (2002) Noninvasive diagnostic tool for inflammation-induced oxidative stress using electron spin resonance spectroscopy and an extracellular cyclic hydroxylamine, *Arch. Biochem. Biophys. 402*, 218−226.
38. Palazzolo, A. M., Suquet, C., Konkel, M. E., and Hurst, J. K. (2005) Green fluorescent protein-expressing *Escherichia coli* as a selective probe for HOCl generation within neutrophils, *Biochemistry 44*, 6910−6919.
39. Jiang, Q., and Hurst, J. K. (1997) Relative chlorinating, nitrating, and oxidizing capabilities of neutrophils determined with phagocytosable probes, *J. Biol. Chem. 272*, 32767−32772.
40. Lymar, S. V., Jiang, Q., and Hurst, J. K. (1996) Mechanism of carbon dioxide-catalyzed oxidation of tyrosine by peroxynitrite, *Biochemistry 35*, 7855−7861.
41. Hurst, J. K., Albrich, J. M., Green, T. R., Rosen, H., and Klebanoff, S. J. (1984) Myeloperoxidase-dependent fluorescein chlorination by stimulated neutrophils, *J. Biol. Chem. 259*, 4812−4821.
42. Ohkuma, S., and Poole, B. (1978) Fluorescence probe measurements of the intralysosomal pH in living cells and the perturbation of pH by various agents, *Proc. Natl. Acad. Sci. U.S.A. 75*, 3327−3331.
43. Elzanowska, H., Wolcott, R. G., Hannum, D. M., and Hurst, J. K. (1995) Bactericidal properties of hydrogen peroxide and copper or iron-containing complex ions in relation to leukocyte function, *Free Radical Biol. Med. 18*, 437− 449.
44. Zhao, H., Joseph, J., Fales, H. M., Sokoloski, E. A., Levine, R. L., Vasquez-Vivar, J., and Kalyanaraman, B. (2005) Detection and characterization of the product of hydroethidine and intracellular superoxide by HPLC and limitations of fluorescence, *Proc. Natl. Acad. Sci. U.S.A. 102*, 5727−5732.
45. Cohen, H. J., and Chovaniec, M. E. (1978) Superoxide generation by digitonin-stimulated guinea pig granulocytes. A basis for a continuous assay for monitoring superoxide production and for the study of the activation of the generating system, *J. Clin. Invest. 61*, 1081−1087.
46. Makino, R., Tanaka, T., Iizuka, T., Ishimura, Y., and Kanegasaki, S. (1986) Stoichiometric conversion of oxygen to superoxide anion during the respiratory burst in neutrophils, *J. Biol. Chem. 261*, 11444−11447.
47. Hurst, J. K., and Barrette, W. C., Jr. (1989) Leukocyte oxygen activation and microbicidal oxidative toxins, *CRC Crit. Rev. Biochem. Mol. Biol. 24*, 271−328.
48. Lymar, S. V., Khairutdinov, R. F., and Hurst, J. K. (2003) Hydroxyl radical formation by O-O bond homolysis in peroxynitrous acid, *Inorg. Chem. 42*, 5259−5266.
49. Lymar, S. V., Shafirovich, V., and Poskrebyshev, G. A. (2005) One-electron reduction of aqueous nitric oxide: a mechanistic revision, *Inorg. Chem. 44*, 5212−5221.
50. Morel, F., Doussiere, J., and Vignais, P. V. (1991) The superoxide-generating oxidase of phagocytic cells. Physiological, molecular and pathological aspects, *Eur. J. Biochem. 201*, 523−546.
51. Iyengar, R., Stuehr, D. J., and Marletta, M. A. (1987) Macrophage synthesis of nitrite and N-nitrosamines: precursors and role of the respiratory burst. *Proc. Natl. Acad. Sci. U.S.A. 84*, 6369−6373.
52. Stuehr, D. J., Pou, S., and Rosen, G. M. (2001) Oxygen reduction by nitric oxide synthases, *J. Biol. Chem. 276*, 14533−14536.
53. Lopes, de Menezes, S., and Augusto, O. (2001) EPR detection of glutathionyl and protein-tyrosyl radicals during interaction of peroxynitrite with macrophages (J774), *J. Biol. Chem. 276*, 39879−39884.
54. Hurst, J. K. (2002) Whence nitrotyrosine? *J. Clin. Invest. 109*, 1287−1289.
55. Anbar, M., and Taube, H. (1954) Interaction of nitrous acid with hydrogen peroxide, *J. Am. Chem. Soc. 76*, 6243−6247.
56. Lukacs, G. L., Rotstein, O. D., and Grinstein, S. (1990) Phagosomal acidification is mediated by a vacuolar-type H^+-ATPase in murine macrophages, *J. Biol. Chem. 265*, 21009−21107.
57. Lukacs, G. L., Rotstein, O. D., and Grinstein, S. (1991) Determinants of the phagosomal pH in macrophages. *In situ* assessment of the vacuolar H^+-ATPase activity, counterion conductance, and H^+ "leak", *J. Biol Chem. 266*, 24540−24548.
58. Lee, S. H., Soyoola, E., Chanmugam, P., Hart, S., Sun, W., Zhong, H., Liou, S., Simmons, D., and Hwang, D. (1992) Selective expression of mitogen-inducible cyclooxygenase in macrophages stimulated with lipopolysaccharide, *J. Biol. Chem. 267*, 25934−25938.
59. O'Sullivan, M. G., Chilton, F. H., Huggins, E. M., Jr., and McCall, C. E. (1992) Lipopolysaccharide priming of alveolar macrophages for enhanced synthesis of prostanoids involves induction of a novel prostaglandin H synthase, *J. Biol. Chem. 267*, 14547−14550.
60. Fu, J., Masferrer, J. L., Seibert, K., Raz, A., and Needleman, P. (1990) The induction and suppression of prostaglandin H_2 synthase (cyclooxygenase) in human monocytes, *J. Biol. Chem. 265*, 16737−16740.
61. Treinin, A., and Hayon, E. (1970) Absorption spectra and reaction kinetics of NO_2, N_2O_3, and N_2O_4 in aqueous solution, *J. Am. Chem. Soc. 92*, 5821−5828.
62. Seaver, L. C., and Imlay, J. A. (2001) Hydrogen peroxide fluxes and compartmentalization inside growing *Escherichia coli*, *J. Bacteriol. 183*, 7182−7189.
63. Makino, N., Sasaki, K., Hashida, K., and Sakakura, Y. (2004) A metabolic model describing the H_2O_2 elimination by mammalian cells including H_2O_2 permeation through cytoplasmic and peroxisomal membranes; comparison with experimental data, *Biochim. Biophys. Acta 1673*, 149−159.
64. Maehly, A., and Chance, B. (1955) The assay of catalases and peroxidases, *Methods Biochem. Anal. 1*, 357−424.
65. Kristie, D., and Thompson, J. E. (1989) Inhibition of lipoxygenase activity: a cautionary note, *Phytochemistry 28*, 2577−2581.
66. Swindle, E. J., Metcalfe, D. D., and Coleman, J. W. (2004) Rodent and human mast cells produce functionally significant intracellular reactive oxygen species but not nitric oxide, *J. Biol. Chem. 279*, 48751−48759.
67. Swindle, E. J., Coleman, J. W., and Metcalfe, D. D. (2005) Production of reactive oxygen species in both human and mouse mast cells is lipoxygenase-dependent and plays a faciitatory role in antigen mediated cytokine secretion, *Free Radical Biol. Med. 39*, S54.
68. Swindle, E. J., Deleo, F. R., and Metcalfe, D. D. (2006) Production of reactive oxygen species by mast cells following FcγrR aggregation is 5-lipoxygenase- and cyclooxygenase-dependent and NADPH oxidase-independent, *Free Radical Biol. Med. 41*, S76.
69. Keyer, K., Gort, A. S., and Imlay, J. A. (1995) Superoxide and the production of oxidative DNA damage, *J. Bacteriol. 177*, 6782−6790.
70. Klebanoff, S. J. (1993) Reactive nitrogen intermediates and antimicrobial activity: Role of nitrite, *Free Radical Biol. Med. 14*, 351−360.
71. Rouzer, C. A., and Marnett, L. J. (2003) Mechanism of free radical oxygenation of polyunsaturated fatty acids by cyclooxygenases, *Chem. Rev. 103*, 2239−2304.
72. Brash, A. R. (1999) Lipoxygenases: Occurrence, functions, catalysis, and acquisition of substrate, *J. Biol. Chem. 274*, 23679−23682.
73. Kim, S. F., Huri, D. A., and Snyder, S. H. (2005) Inducible nitric oxide synthase binds, S-nitrosylates, and activates cyclooxygenase-2, *Science 310*, 1966−1970.
74. Gunther, M. R., Hsi, L. C., Curtis, J. F., Gierse, J. K., Marnett, L. J., Eling, T. E., and Mason, R. P. (1997) Nitric oxide trapping of the tyrosyl radical of prostaglandin H synthase-2 leads to tyrosine iminoxyl radical and tyrosine formation, *J. Biol. Chem. 272*, 17086−17090.

BI700123S